






RESEARCH ARTICLE | MAY 09 2023

Strouhal and Reynolds number scaling of force production in the Mountain Pine Beetle

Zahra Hajati ; Antonia Musso ; Zachary Weller ; Maya Evenden ; Jaime G. Wong 



Physics of Fluids 35, 057111 (2023)

<https://doi.org/10.1063/5.0145208>

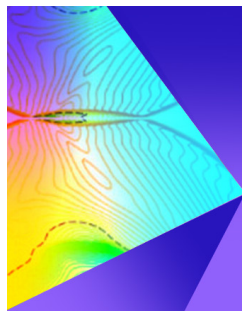


View
Online



Export
Citation

CrossMark



Physics of Fluids

Special Topic: Shock Waves

Submit Today!

Strouhal and Reynolds number scaling of force production in the Mountain Pine Beetle

Cite as: Phys. Fluids **35**, 057111 (2023); doi: [10.1063/5.0145208](https://doi.org/10.1063/5.0145208)

Submitted: 3 February 2023 · Accepted: 31 March 2023 ·

Published Online: 9 May 2023



View Online



Export Citation



CrossMark

Zahra Hajati,^{1,a)}  Antonia Musso,²  Zachary Weller,²  Maya Evenden,²  and Jaime G. Wong¹ 

AFFILIATIONS

¹Department of Mechanical Engineering, University of Alberta, Edmonton, Alberta T6G 1H9, Canada

²Department of Biological Sciences, University of Alberta, Edmonton, Alberta T6G 2E9, Canada

^{a)} Author to whom correspondence should be addressed: hajati@ualberta.ca

ABSTRACT

The Mountain Pine Beetle, *Dendroctonus ponderosae* Hopkins (Coleoptera: Curculionidae: Scolytinae), a destructive pest found in the pine forests of Western North America, has exhibited range expansion and unprecedented population growth due to climate change. As this insect disperses by flight, understanding its flight mechanics may help to model and predict its rate of spread through the environment. In this work, aerodynamic scaling relationships—previously identified in idealized, predominantly two-dimensional and numerical cases—are applied to the case of live flight. In particular, this aims to improve the statistical confidence in predicting sex and age differences in flight performance, which have historically been analyzed in ecology using dimensional quantities. Thrust coefficient is found to scale with the square of Strouhal number, as has been found in prior studies. However, with respect to Reynolds number, scaling was with the inverse of Reynolds number, rather than the inverse of the square root. We demonstrate here that the established Strouhal number and Reynolds number scaling of force coefficient can be successfully extended not just to highly three-dimensional flows, and lower Reynolds number flows, but remains robust even across distinct individuals within a population of beetles. Using this scaling, we observe that males fly with a greater mean thrust coefficient and Strouhal number compared to females ($p < 0.001$), which is a significant improvement in statistical confidence over prior studies, which could not identify a major difference between sexes ($p > 0.05$). Meanwhile, there is also a significant difference in thrust coefficient between different age cohorts, with younger beetles exhibiting a lower magnitude than other age groups ($p < 0.05$).

Published under an exclusive license by AIP Publishing. <https://doi.org/10.1063/5.0145208>

I. INTRODUCTION

The Mountain Pine Beetle (MPB), *Dendroctonus ponderosae* Hopkins (Coleoptera: Curculionidae: Scolytinae), is one of the main causes of tree mortality in the pine forests of North America. The lodgepole pine is one of the most effected species being infested by the MPBs (Negrón and Huckaby, 2020). The continued population growth and spread of the Mountain Pine Beetle (MPB) in pine forests of Western North America is driven in large part by climate change. The increasing population of this insect has led to the mortality of thousands of hectares of pine forests in British Columbia (Safranyik *et al.*, 2007), and it has expanded its range into Alberta in proximity to the boreal forest (Cullingham *et al.*, 2011). As a result, these areas are more vulnerable to wildfire and may therefore be a source of carbon emissions from the burned or decaying wood of the dead trees (Kumar *et al.*, 2008). Increased tree mortality has resulted in Canada's forests becoming a large net source of atmospheric carbon dioxide, rather than a sink (Hurteau, 2021). These increases in carbon emissions (or decreased carbon uptake) will accelerate climate change and,

consequently, feedback to result in further outbreaks of the beetle population (Embrey *et al.*, 2012).

The MPB disperses by flight, contributing to its spread through the environment (see, e.g., Carroll *et al.*, 2003). It is critical to understand the flight performance of the MPB in order to better estimate its spread through the environment and to preserve pine species in the boreal forest. For instance, Evenden *et al.* (2014) studied the effect of body weight, fat content, and beetle age on flight endurance. It was found that both the larger and younger beetles are more likely to fly and that they flew longer distances and durations compared to the smaller beetles and older ones ($p < 0.05$). However, they found no direct effect of beetle sex on their flight capacity ($p > 0.05$). Due to the inherent noise found in biological data, however, it is unclear if there is truly no correlation between flight endurance and range with sex, or if the correlation is merely difficult to observe due to confounding variables. In particular, many prior studies on MPB flight have focused on determining flight characteristics based on dimensional parameters. Whereas dimensionless scaling is routine in fluid mechanics,

it is relatively rare in ecological studies, and so we propose that this may be a mechanism to improve correlation quality in ecological studies, and for the MPB in particular.

In flapping propulsion, the Strouhal number St is a critical dimensionless parameter, which can be interpreted as a dimensionless amplitude of the flapping motion:

$$St = \frac{(2h)f}{U}, \tag{1}$$

where h is the flapping amplitude, f is the flapping frequency, and U is the free-stream velocity, or flight velocity in our case. The Strouhal number represents the ratio of the vertical distance the wing travels up and down during a cycle of motion, $2h$, to the forward distance traversed over same time interval, U/f . This simple aspect ratio of the wave traced by a moving airfoil encodes significant information about the force production and the efficiency of thrust production. For instance, Triantafyllou *et al.* (1991) found that the optimum efficiency of the foil occurs within the Strouhal range of 0.25 and 0.35. Taylor *et al.* (2003) found that the highest propulsive efficiency of all the flying or swimming animals occurs in the same narrow range of $0.2 < St < 0.4$ when cruising and that this convergence was sufficiently pronounced to be used as a predictive tool.

This Strouhal number range corresponds with the so-called optimal vortex formation (see Dabiri, 2009), intrinsically tying this efficiency to circulation generation in the vortices in the flow. The significance of the Strouhal number can thus also be attributed to its relationship with circulation generation. For instance, when an airfoil undergoes rapid pitching, it can produce a large coherent vortex known as a leading-edge vortex (LEV). Pitt Ford and Babinsky (2013) showed that the LEV is the dominant contributor to circulation in insect-scale unsteady motions. Baik *et al.* (2012) suggested that while the Strouhal number of a pitching and heaving airfoil determined its force production, the reduced frequency had a greater influence over the topology of the LEV. Here, the reduced frequency has a very similar definition to the Strouhal number

$$k = \frac{\pi fc}{U}, \tag{2}$$

where c is the chord of the airfoil. Whereas the Strouhal number can be interpreted as a ratio of length scales, we can interpret the reduced frequency as a ratio of timescales: the convective timescale, c/U , vs the timescale of motion, $1/f$.

Given the established relationship between Strouhal number and force production, and the dominant role of the LEV in circulation generation at low Reynolds numbers, we can expect that the relationship between Strouhal number and force production is mediated by the circulation of this LEV. For instance, consider the model of von Karman and Sears (1938)

$$L = -\rho \frac{d}{dt} \sum \Gamma_i x_i, \tag{3}$$

where L is the lift, ρ is the fluid density, and Γ_i and x_i are the circulation and the x -coordinate of the i th vortex, respectively. Under the product rule, we might re-write this equation as

$$L = -\rho \sum (\Gamma_i \dot{x}_i + \dot{\Gamma}_i x_i), \tag{4}$$

where the $\dot{\Gamma}$ term has been previously associated with added mass (for instance, see Mancini *et al.*, 2015), following the description of added

mass by Theodorsen (1935). Several authors have shown that the rate of circulation growth scales with u^2 , in various different contexts. For instance, Morton (1984) found that for a boundary layer, circulation is generated entirely at the leading-edge of the boundary layer at a rate of $\frac{1}{2}U^2$. A similar result was found by Didden (1979) for the rate of circulation growth in the vortex ring generated by a piston-cylinder, while Wong and Rival (2015) showed that the circulation growth of the LEV on a plunging airfoil scaled with u_{eff}^2 .

For a plunging airfoil, this rate of growth u_{eff}^2 can be shown to be proportional to St^2 . For a sinusoidally plunging airfoil, the peak vertical velocity is

$$h = h_0 \sin(2\pi ft) \rightarrow \dot{h}_{\text{max}} = 2\pi fh_0. \tag{5}$$

If we begin with the established relationship for circulation growth

$$\frac{\partial \Gamma}{\partial t} \propto u_{\text{eff}}^2, \tag{6}$$

we can non-dimensionalize this expression by the free-stream velocity and expand u_{eff} , as shown by Wong (2017), to show that

$$\frac{\partial \Gamma}{\partial t} \frac{1}{U_\infty^2} \propto \frac{u_{\text{eff}}^2}{U_\infty^2} = \frac{(2\pi fh_0)^2 + U_\infty^2}{U_\infty^2} = \pi^2 St^2 + 1. \tag{7}$$

This suggests that we can expect the $\dot{\Gamma}$ component of lift, which can be interpreted as an added mass term, to scale proportional to St^2 . Indeed, the entire thrust coefficient has been identified to scale in this way such as by Floryan *et al.* (2017). For instance, Senturk and Smits (2019) gives the following scaling for thrust coefficient:

$$C_T = \beta St^2 - C_D, \tag{8}$$

where β takes the form

$$\beta = \beta_0 + \alpha Re^{-0.5}, \tag{9}$$

and the drag coefficient takes the form

$$C_D = C_{D,0} + \gamma Re^{-0.5}, \tag{10}$$

where β_0 , $C_{D,0}$, α , and γ are constant scalar coefficients. Given appropriate values for these coefficients, the resulting scaling of C_T with St^2 is exceptionally linear, with very little noise. This model was produced by Senturk and Smits (2019) in the context of idealized, two-dimensional NACA 0012 airfoils, with further results compiled numerically (see, e.g., Mallah *et al.*, 2021). A similar laminar scaling as Eq. (10) was studied by Verma *et al.* (2022) and found to work for a two-dimensional teardrop airfoil with pitching and heaving motion. This scaling was found accurate for the angles of attack below 20, but less accurate at higher reduced frequencies and amplitudes. The prior studies are conducted for two-dimensional or spanwise periodic cases and proposed a scaling with $Re^{-0.5}$, due to the Blasius solution which assumes a 2D boundary layer (Yu and Huang, 2021), while in the current study, we propose that the above model may adequately robust to model three-dimensional insect flight, and we attempt to apply it to the flight kinematics of live MPB. In particular, we hypothesize that sex and age differences in the flight performance of the MPB can be determined at a significantly greater statistical confidence than traditional methods by utilizing the above form of dimensional analysis.

There are a number of possible confounding variables in this process. In particular, we investigate 3D wings instead of 2D airfoils.

Moreover, a simple reality of biological measurements is that no two “airfoils” (the membrane-wings of individual insects) in the current study will be identical (certainly nowhere near the repeatability of numerically defined NACA profiles). As such, this will also be a test of the robustness of the above model. Moreover, as the Reynolds number of MPB flight is substantially lower than explored by [Senturk and Smits \(2019\)](#)—we will be investigating cases on the order of $Re \approx 10^2$, whereas they spanned $Re \approx 10^3$ – 10^5 —we will also consider the possibility that force coefficients scale linearly with Reynolds number instead of with the square root. That is,

$$C_D \propto \frac{1}{Re}. \tag{11}$$

In order to assess this model in the context of live insect flight, we must have both a method to measure the forces produced by an insect in flight and to measure its wing kinematics. These methods are discussed in Sec. II.

II. METHODS

In this study, MPB are tethered to a device known as a flight mill, shown schematically in [Fig. 1](#), to enable simultaneous measurement of force generation and wing kinematics. This is a common tool in entomology in long-duration flight studies, to measure flight distances by counting rotations. A general background on design and operation of a flight mill can be found in [Ribak et al. \(2017\)](#). Using this tool, insects are suspended from a rotating pivot, restricting their flight to a circular path. As the insect repeats the same path in every rotation about the flight mill, a fixed camera can reliably capture their motion at high resolution. However, it is not clear how a flight mill impacts the real flight behavior of an insect (see, e.g., [Williams and Robertson, 2008](#); [Jactel and Gaillard, 1991](#)). For instance, various researchers suggest that flight performance may be either improved, by eliminating the need for the insect to support its own body weight, or impaired, by forcing the insect to overcome the additional drag of the flight mill itself (for instance, [Riley et al., 1997](#); [Robertson and Roitberg, 1998](#)). While the force estimation techniques discussed here may be helpful in

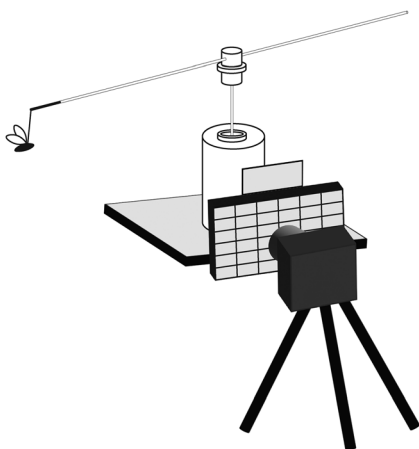


FIG. 1. The flight mill and the camera setup used for the experiments. A calibration target can be placed tangent to the insect flight path in order to convert the camera-scale to the lab-scale and extract the flight kinematics.

addressing this debate, we will not explicitly address the issue here. Rather, we merely aim to compare the force the beetles produce to their wing kinematics in confined flight, without concern if this accurately reflects natural flight in the wild, which we leave to specialists in entomology. High-speed imaging is used to capture individual wing-beat kinematics, while the friction of the flight mill itself is used to determine the net force generated by the insects in flight. The friction estimation of the flight mill is discussed in Sec. II A.

A. Flight mill friction calibration

The net force (thrust less aerodynamic drag) produced by the insect, along its constrained flight path, must be equal to the net friction force of the flight mill. Therefore, in order to measure force coefficients of insects in flight, the coefficient of friction must be calibrated. This coefficient of friction can be determined by observing the rate of decay of the apparatus upon an impulsive start, under the influence of friction alone. If we assume that friction is dominated by viscous effects, the governing equation of motion is

$$I\ddot{\theta} + B\dot{\theta} = 0, \tag{12}$$

where θ is the absolute angle of the flight mill, I is the moment of inertia, and B is the unknown coefficient of friction that we wish to measure. The classical solution to Eq. (12) is

$$\dot{\theta} = \dot{\theta}_0 e^{-bt}, \tag{13}$$

where $\dot{\theta}_0$ is the initial velocity, and b is the decay rate. If the angle of the flight mill is captured as a function of time during free decay, then the coefficient b can be determined by curve fitting. Substituting this solution back into Eq. (12), the coefficient of friction is given by $B = -Ib$. In a steady forward flight, the product of the coefficient of the friction and the angular velocity of the mill is therefore balanced by the net thrust coefficient, $C_T - C_D$, that is produced by the insect in their flight.

To measure velocity decay of our flight mill, overhead video captured with a standard commercial webcam (Logitech Inc., Lausanne, Switzerland) was used to measure the angular position of the mill over time, and this angle was extracted from the video frames with a MATLAB script developed in-house (MathWorks Ltd., MA, USA), which is included in the supplementary material. This process was repeated for 25 initiations such that an uncertainty estimate of the friction coefficient could be produced. All 25 velocity decay curves can be seen plotted in [Fig. 2](#), showing that at high speeds (that is, early in the velocity decay toward the left-hand side of the plot), a single decay rate is shared among all initiations regardless of the initial velocities. Each run eventually deviates from this common decay rate curve at a different time, based on its initial velocity, with slower initial velocities deviating earlier.

As the beetle maintains high velocities relative to the point of deviation in these decay curves—in other words, because beetle velocities correspond to the far left-hand side of [Fig. 2](#)—the assumption that viscous friction dominates the resistance of the flight mill produces very little error. This methodology resulted in an estimate of the friction coefficient as $B = 1.03 \times 10^{-6} \text{ N m s/rad}$, with an uncertainty of $\sigma_B = 6 \times 10^{-8} \text{ N m s/rad}$, or approximately 5.5%.

However, because this technique can only measure *net* thrust, two considerations must be made. First, we may wish to slightly modify the relationship derived by [Senturk and Smits \(2019\)](#)

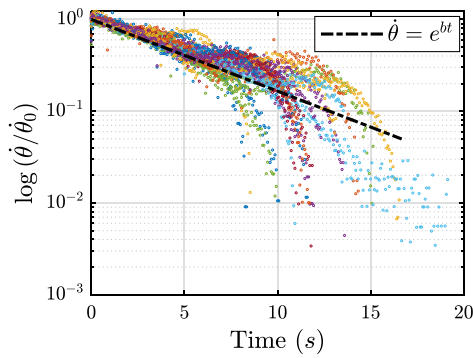


FIG. 2. Velocity decay curves for 25 different impulsive start velocities. Toward the left-hand side of the plot, we can see that all 25 initiations share the same decay rate, indicating that this is the system's coefficient of friction.

$$C_T - C_D = \beta St^2 \rightarrow C_T = \beta St^2 + C_D, \tag{14}$$

where β and C_D are as follows:

$$\beta = \beta_0 + \frac{\alpha}{Re} \tag{15}$$

and

$$C_D = C_{D,0} + \frac{\gamma}{Re}. \tag{16}$$

This change of sign in C_D does not alter our methodology but does ensure that the sign of our derived coefficients that will be determined below in Sec. III imply a positive drag coefficient. Second, we must ensure that the thrust coefficient of the beetles are directed in the direction of motion along the path of the flight mill, which is described in Sec. II B.

B. Wake direction measurements

Equation (12) is used to calibrate the forces in the circumferential direction of flight only. As such, we must determine that the direction of thrust production by the beetle is primarily in this direction of motion, such that the calibrated force measured on the flight mill is balanced by the total force generation of the beetle. To do so, beetles were mounted to the flight mill at various body angles, and the resulting fluid jet behind the beetle was measured using Particle Image Velocimetry (PIV), using the experimental setup shown schematically in Fig. 3.

For these measurements, the flow was seeded with water-glycol microdroplets from a commercial fog machine and illuminated with a 5-W ($\lambda = 532$ nm) continuous-wave laser. The flow-field was captured with a Photron Fastcam WX-50 high-speed camera (Photron Inc., Tokyo, Japan) and processed in LaVision Davis 10 (LaVision GmbH, Göttingen, Germany). As the purpose of the PIV images was to determine the angle of the jet produced by the beetles, extensive error analysis will be omitted here. Rather, this setup was used to determine the jet angles produced by various insect mounting positions, with two extreme cases exemplified by Figs. 4(a) and 4(b). Note the tether angle (the metal wire used to fix the beetles to the flight mill, illuminated brightly as the vertical line above the beetle's body in Fig. 4) determines the jet angle. As the jet angle shown in Fig. 4(a) was

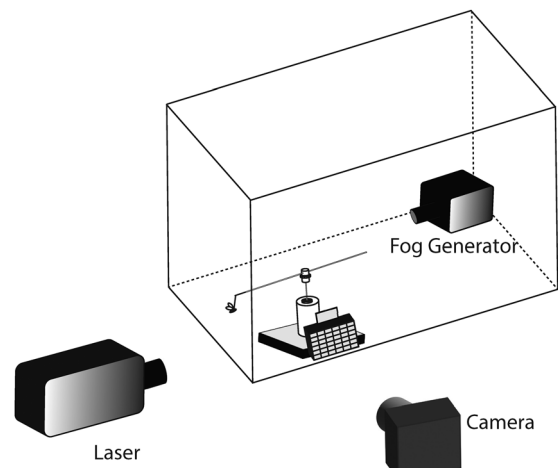


FIG. 3. The PIV setup used to compute the wake jet angle. The rectangular prism surrounding the flight mill represents a glass-walled tank used to contain the seeding media, which was produced by a fog machine. A laser sheet was generated tangent to the flight path of the beetle, with the laser plane normal to the camera axis.

deemed reasonably close to horizontal, and therefore parallel with the direction of motion, that body angle was used for all further tests, such as the flight kinematics measurements described below by repeating the tether angle and body-tether mounting procedure used for that test case.

C. Flight kinematics extraction

Flights of individual MPB were captured with the same WX-50 high-speed camera used to capture PIV images, at a 20 482 048 px² resolution and 12-bit monochrome bit-depth. For the capture of flight kinematics, an image magnification of approximately 0.2 is achieved with a 100 mm/2.8 macro lens (Tamron Co., Saitama, Japan), resulting in a resolution of approximately 50 μ m per pixel. The path of the flight mill was arranged tangential to a printed grid of uniform 1 cm spacing, which was used to calibrate a scale conversion between image-scale and lab-scale (i.e., from pixels to millimeters). The deviation of the grid was verified by caliper and optically to within 50 μ m. It is likely that the resolution of the target was better than this value, given typical resolutions provided by commercial printers. However, 50 μ m was the limit of verification imposed by calipers.

An in-house image processing software written in MATLAB (MathWorks Ltd., MA, USA), also provided in the supplementary material, was used to extract wing-tip position and dimensions from the calibrated high-speed video data, as illustrated in Fig. 5. The wing-tip position over time was used to compute flapping amplitude and frequency, as well as the mean forward velocity, averaged over several wing-beat cycles. Both Strouhal number and Reynolds number can be extracted from the wing-beat frequency, amplitude, and forward velocity, while the net thrust can be determined from the forward velocity via angular velocity and our established coefficient determined above. These flight parameters were extracted for 165 individual flights of 38 individual beetles, divided between 17 males and 21 females in four different age cohorts (0–2, 3–5, 6–8, and 9–10 days post-emergence,

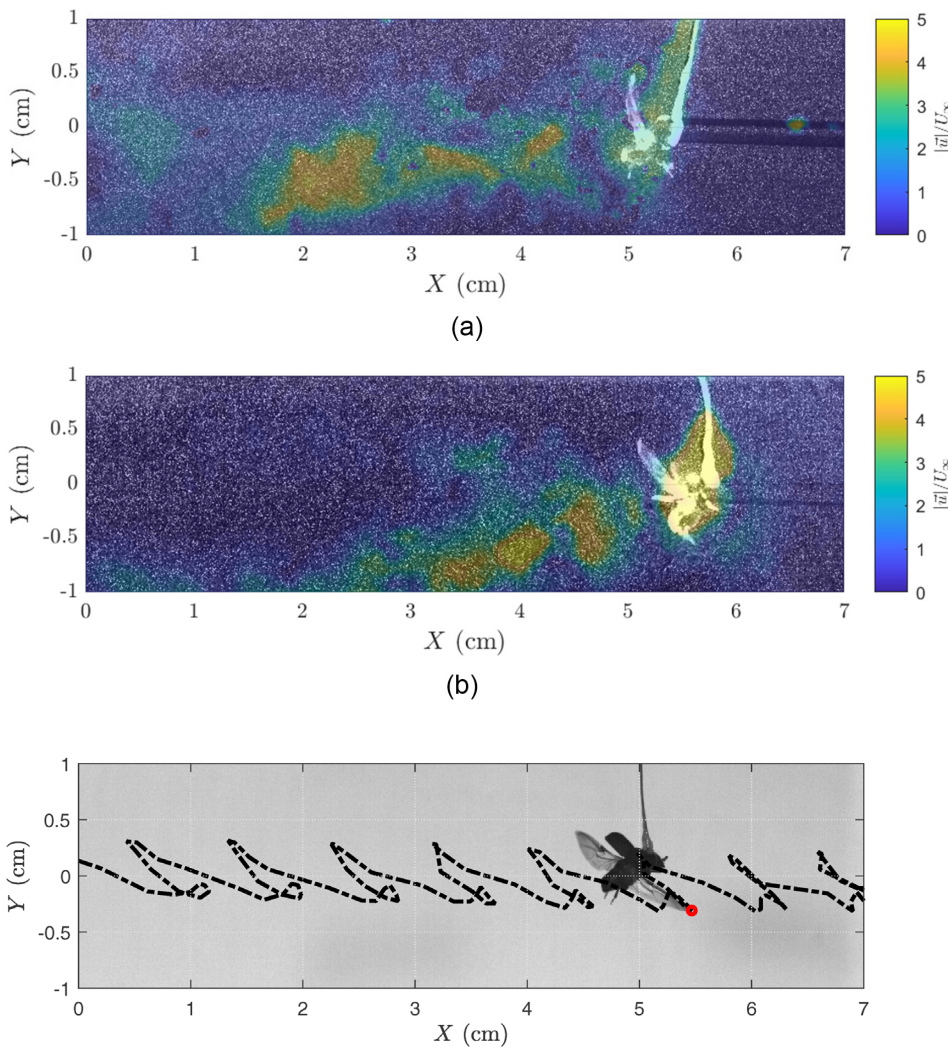


FIG. 4. A comparison of fluid jet generated behind beetles at two different tether angles, as computed with PIV shows that the resulting jet angle is determined by the tether angle. The first tether angle, 260° , was used throughout the tests here. (a) A beetle mounted with a tether angle of approximately 260° relative to forward motion (10° less than vertical). (b) A beetle mounted with a tether angle of approximately 280° relative to forward motion (10° past vertical).

FIG. 5. The path traced by the tip of the beetle's wing is extracted from a high-speed video, shown here overlaid against a raw image of the beetle in flight. The frequency and amplitude of motion can be extracted by Fourier transform, while the forward velocity is estimated by the mean forward velocity of this wingtip.

respectively), in order to test the hypotheses that sex and age differences in flight performance can be determined at a greater statistical confidence by utilizing dimensional analysis.

III. RESULTS AND DISCUSSION

In this section, we apply the scaling relationship presented in Sec. I to the flight of live insects. Moreover, we demonstrate that this model is able to discriminate differences in flight performance, based on both sex and age differences, at much greater statistical confidence than is possible with traditional ecological techniques. However, we will not attempt to draw any ecological conclusions here, which we leave to future studies dedicated to that topic. Beetles were observed flying in a broad range of Strouhal numbers ($1 \leq St \leq 11$), with a mean value of $St_{\text{mean}} = 3.2$, while the corresponding mean thrust coefficient was $C_{T,\text{mean}} = 1.6$. This is approximately an order of magnitude greater than that observed by Taylor *et al.* (2003) in cruising conditions, and well beyond the peak efficiency identified by Triantafyllou *et al.* (1991), despite the fact that this was under steady conditions.

This is suggestive that the beetles were expending a large amount of energy to produce the high thrust coefficients required to overcome the drag of the apparatus (or, possibly, to attempt escape).

A naive comparison of Strouhal number and thrust coefficient is presented in Fig. 6(a). While there appears to be some underlying correlation, it is also apparent that this correlation is not strong. However, when the Reynolds number scaling suggested by Senturk and Smits (2019) is first modified to use a linear Reynolds number relationship and then applied to this flight data, correlation quality is improved dramatically. Using a simple gradient descent method, the empirical parameters β_0 , $C_{D,0}$, α , and γ in Eqs. (16) and (15) can be determined, resulting in the relationship shown in Fig. 6(b). This shows that, even though the beetles observed in this study flew in the narrow Reynolds number range of $20 \leq Re \leq 150$, it is still critical to account for Reynolds number variation in order to produce a reasonable scaling of force coefficient. The exact numerical results for the empirical coefficients are shown in Table II, and the coefficient of determination of the resulting model is $R^2 = 0.98$. It is worth noting that the modified

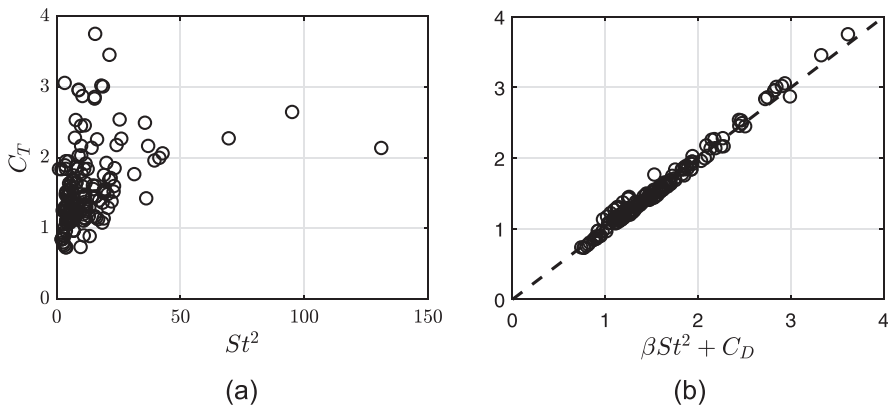


FIG. 6. The thrust coefficient of the beetles vs St^2 and estimated by the scaling relationship. (a) The thrust coefficient vs St^2 of all beetles. (b) The thrust coefficient vs St^2 of all beetles, accounting for Reynolds number scaling.

linear scaling of β and C_D with Reynolds number, $1/Re$ produced a better coefficient of determination than a square-root scaling $1/\sqrt{Re}$. Moreover, it is worth repeating that the individual data points shown in Fig. 6(b) represent 38 different individual beetles of both sexes, and of four different age groups. That is to say, despite the fact that each has a slightly different wing span, wing chord, overall wing shape, body mass, and different fat stores, a single model is able to collapse all individual flights onto a single functional relationship, even though that model was developed in the context of idealized two-dimensional airfoils. In Secs. III A and III B, we will divide these data into subsets in order to identify differences in flight behavior by sex and age cohort.

A. Sex differences

The data previously presented in Fig. 6 are shown now broken down by beetle sex in Fig. 7. Whereas previous flight mill studies were unable to observe significant differences between male and female flight performance ($p > 0.05$), when broken down by the non-dimensional scaling proposed here, we are able to show that males fly with both a greater Strouhal number ($p < 0.001$) and a greater thrust coefficient ($p < 0.001$), with a mean value of $C_T = 1.70$ for males and $C_T = 1.40$ for females in our sample population. The results of the t -test of St and C_T of male and females can be found in Table I.

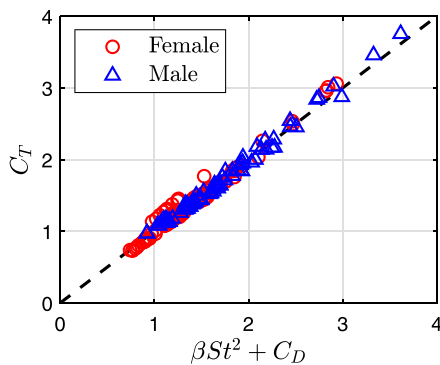


FIG. 7. The thrust coefficient of the beetles estimated by the scaling relationship and divided by sex.

Presenting the distributions of Strouhal number and thrust coefficient as a violin plot in Fig. 8, sex differences in Strouhal number and thrust coefficient are apparent even without this regression. However, the full scaling relationship may provide predictive power in ecological studies, such as estimating range or endurance (i.e., long timescale flight behavior) from short observations of a handful of wingbeats. For instance, by performing the gradient descent process on each sex group independently, we are able to show that the thrust coefficient of male beetles scales more quickly with both Strouhal number and Reynolds number, as shown in Table II.

B. Age differences

In this section, we study and compare the thrust coefficient and Strouhal number of the MPB based on their age. The data shown in Fig. 6 can be found separated by age in Fig. 9. The probability distribution of mean Strouhal number and thrust coefficient for each age cohort is shown by violin plot in Fig. 10. Previous studies have found that the younger beetles are more likely to fly, and once in flight, fly longer distances and time compared to the older beetles ($p < 0.05$) (Evdenden et al., 2014). This is consistent with our results, as the youngest group of beetles flew with a lower mean thrust coefficient of

TABLE I. t -test of two-samples assuming unequal variances for St and C_T for male and females.

	St		C_T	
	Male	Female	Male	Female
Mean	3.52	2.84	1.70	1.41
Variance	2.03	1.12	0.34	0.26
Observations	76	89	76	89
Hypothesized mean difference	0		0	
df	137		150	
t stat	3.41		3.31	
$P(T \leq t)$ one-tail	0.000 433		0.000 577	
t critical one-tail	3.15		3.15	
$P(T \leq t)$ two-tail	0.000 866		0.001 154	
t critical two-tail	3.36		3.36	

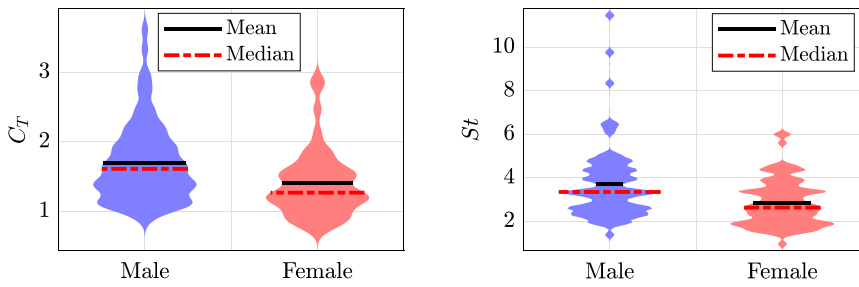


FIG. 8. The mean St and C_T for males and females.

TABLE II. Empirical parameters for Eqs. (15) and (16).

	$C_{D,0}$	γ	β_0	α
Female	0.0317	-91.4468	0.0031	-0.1825
Male	0.0375	-95.1490	0.0057	-0.3740

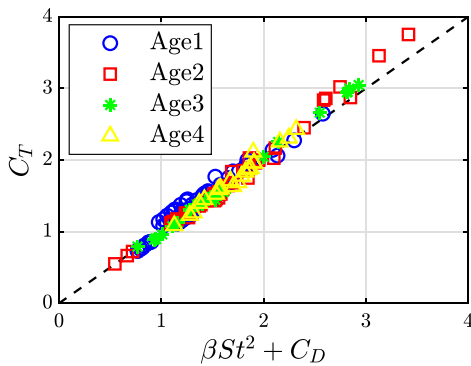


FIG. 9. The thrust coefficient estimated by a scaling relationship for age cohorts.

$C_{T,mean} = 1.33$ compared to all other age groups of the beetles ($p < 0.05$), which corresponds to lower Strouhal numbers and therefore at higher propulsive efficiency.

Comparing the results in Fig. 10 shows that there is a significant difference between the Strouhal number of the youngest group (i.e., $St = 3.4$) compared to all the other age cohorts ($p < 0.001$).

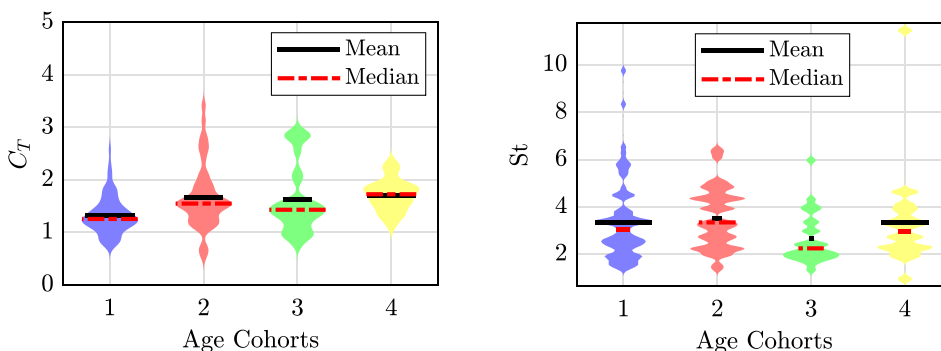


FIG. 10. The mean St and C_T for age cohorts.

IV. CONCLUSIONS

In this study, we have modified an existing scaling relationship between thrust coefficient, Strouhal number, and Reynolds number to apply to low-Reynolds number, three-dimensional wings. Using this modified scaling relationship, we have dramatically improved statistical confidence in sex and age differences previously observed in entomological studies. This methodology required determination of the friction coefficient of a flight mill, and this method can be extended to the other apparatus as well. This model is extremely robust and is able to not only identify the scaling of a three-dimensional wing, but the scaling between *different* three-dimensional wings belonging to distinct individual animals.

This study showed that there are differences in both thrust coefficient C_T and Strouhal number between male and female beetles to a very high degree of confidence ($p < 0.001$) and that males fly with a greater mean thrust coefficient C_T and Strouhal number compared to females. This implies that females may have greater endurance than males, as the Strouhal numbers observed here are well above that required for peak propulsive efficiency. It is also found that there is a significant difference in thrust coefficient C_T with respect to age cohorts, where younger beetles fly with a lower thrust coefficient C_T than the other age cohorts ($p < 0.05$), which is in agreement with the previous findings of Evenden *et al.* (2014). The first age cohort significantly differs in their Strouhal numbers compared to all other age cohorts ($p < 0.001$).

While the precise numerical relationship between free flight (and especially free flight in the natural environment) and flight tethered to a flight mill is not yet understood, the model presented here may be able to improve flight-mill studies in the future. It may be possible to use a model like the one presented here to relate the long-timescale flights by beetles (on the order of hours) to the short-timescale flight behavior of wingbeats, in order to better describe energy expenditure and therefore better predict range and endurance.

Downloaded from http://pubs.aip.org/aip/pof/article-pdf/doi/10.1063/5.0145208/17379500/057111_1_5.0145208.pdf

AUTHOR DECLARATIONS

Conflict of Interest

The authors have no conflicts to disclose.

Author Contributions

Zahra Hajati: Formal analysis (equal); Investigation (equal); Writing – original draft (equal). **Antonia Musso:** Data curation (equal). **Zachary Weller:** Data curation (equal). **Maya Evenden:** Project administration (equal); Writing – review & editing (equal). **Jaime G. Wong:** Formal analysis (equal); Investigation (equal); Project administration (equal); Supervision (equal); Writing – original draft (equal).

DATA AVAILABILITY

The data that support the findings of this study are available from the corresponding authors upon reasonable request.

REFERENCES

- Baik, Y. S., Bernal, L. P., Granlund, K., and Ol, M. V., “Unsteady force generation and vortex dynamics of pitching and plunging aerofoils,” *J. Fluid Mech.* **709**, 37–68 (2012).
- Carroll, A. L., Safranyik, L. *et al.*, “The bionomics of the mountain pine beetle in lodgepole pine forests: Establishing a context,” in Mountain Pine Beetle Symposium: Challenges and Solutions, 2003.
- Cullingham, C. I., Cooke, J. E., Dang, S., Davis, C. S., Cooke, B. J., and Coltman, D. W., “Mountain pine beetle host-range expansion threatens the boreal forest,” *Mol. Ecol.* **20**(10), 2157–2171 (2011).
- Dabiri, J. O., “Optimal vortex formation as a unifying principle in biological propulsion,” *Annu. Rev. Fluid Mech.* **41**, 17–33 (2009).
- Didden, N., “On the formation of vortex rings: Rolling-up and production of circulation,” *J. Appl. Math. Phys.* **30**(1), 101–116 (1979).
- Embrey, S., Remais, J. V., and Hess, J., “Climate change and ecosystem disruption: The health impacts of the North American Rocky Mountain pine beetle infestation,” *Am. J. Public Health* **102**(5), 818–827 (2012).
- Evenden, M. L., Whitehouse, C., and Sykes, J., “Factors influencing flight capacity of the mountain pine beetle (Coleoptera: Curculionidae: Scolytinae),” *Environ. Entomol.* **43**(1), 187–196 (2014).
- Floryan, D., Van Buren, T., Rowley, C. W., and Smits, A. J., “Scaling the propulsive performance of heaving and pitching foils,” *J. Fluid Mech.* **822**, 386–397 (2017).
- Hurteau, M. D., “The role of forests in the carbon cycle and in climate change,” in *Climate Change*, 3rd ed., edited by T. M. Letcher (Elsevier, 2021), Chap. 27, pp. 561–579.
- Jactel, H. and Gaillard, J., “A preliminary study of the dispersal potential of *Ips sexdentatus* (Boern) (Col., Scolytidae) with an automatically recording flight mill,” *J. Appl. Entomol.* **112**(1–5), 138–145 (1991).
- Kumar, A., Flynn, P., and Sokhansanj, S., “Biopower generation from mountain pine infested wood in Canada: An economical opportunity for greenhouse gas mitigation,” *Renewable Energy* **33**(6), 1354–1363 (2008).
- Mallah, S. R., Sooraj, P., Sharma, A., and Agrawal, A., “Effect of superhydrophobicity on the wake of a pitching foil across various Strouhal numbers,” *Phys. Fluids* **33**(11), 111905 (2021).
- Mancini, P., Manar, F., Granlund, K., Ol, M. V., and Jones, A. R., “Unsteady aerodynamic characteristics of a translating rigid wing at low Reynolds number,” *Phys. Fluids* **27**(12), 123102 (2015).
- Morton, B., “The generation and decay of vorticity,” *Geophys. Astrophys. Fluid Dyn.* **28**(3–4), 277–308 (1984).
- Negrón, J. F. and Huckaby, L., “Reconstructing historical outbreaks of mountain pine beetle in lodgepole pine forests in the Colorado Front Range,” *For. Ecol. Manage.* **473**, 118270 (2020).
- Pitt Ford, C. P. and Babinsky, H., “Lift and the leading-edge vortex,” *J. Fluid Mech.* **720**, 280–313 (2013).
- Ribak, G., Barkan, S., and Soroker, V., “The aerodynamics of flight in an insect flight-mill,” *PLoS One* **12**(11), e0186441 (2017).
- Riley, J., Downham, M., and Cooter, R., “Comparison of the performance of *Cicadulina* leafhoppers on flight mills with that to be expected in free flight,” *Entomol. Exp. Appl.* **83**(3), 317–322 (1997).
- Robertson, I. C. and Roitberg, B. D., “Duration of paternal care in pine engraver beetles: Why do larger males care less?,” *Behav. Ecol. Sociobiol.* **43**, 379–386 (1998).
- Safranyik, L., Wilson, B. *et al.*, *The Mountain Pine Beetle: A Synthesis of Biology, Management and Impacts on Lodgepole Pine* (Canadian Forest Service, 2007).
- Senturk, U. and Smits, A. J., “Reynolds number scaling of the propulsive performance of a pitching airfoil,” *AIAA J.* **57**(7), 2663–2669 (2019).
- Taylor, G. K., Nudds, R. L., and Thomas, A. L., “Flying and swimming animals cruise at a Strouhal number tuned for high power efficiency,” *Nature* **425**(6959), 707–711 (2003).
- Theodorsen, T., “General theory of aerodynamic instability and the mechanism of flutter,” Report No. 496 (National Advisory Committee for Aeronautics, 1935).
- Triantafyllou, M., Triantafyllou, G., and Gopalkrishnan, R., “Wake mechanics for thrust generation in oscillating foils,” *Phys. Fluids A* **3**(12), 2835–2837 (1991).
- Verma, S., Freeman, B. R., and Hemmati, A., “Effects of Reynolds number and average angle of attack on the laminar scaling of oscillating foils,” *Phys. Fluids* **34**(3), 031905 (2022).
- von Karman, T. H. and Sears, W. R., “Airfoil theory for non-uniform motion,” *J. Aeronaut. Sci.* **5**(10), 379–390 (1938).
- Williams, W. I. and Robertson, I. C., “Using automated flight mills to manipulate fat reserves in Douglas-fir beetles (Coleoptera: Curculionidae),” *Environ. Entomol.* **37**(4), 850–856 (2008).
- Wong, J. G., “Wing kinematics and flexibility for optimal manoeuvring and escape,” Ph.D. thesis (Queen’s University, Canada, 2017).
- Wong, J. G. and Rival, D. E., “Determining the relative stability of leading-edge vortices on nominally two-dimensional flapping profiles,” *J. Fluid Mech.* **766**, 611–625 (2015).
- Yu, Y.-L. and Huang, K.-J., “Scaling law of fish undulatory propulsion,” *Phys. Fluids* **33**(6), 061905 (2021).